Corosolic acid reduces NSCLC cell proliferation, invasion, and chemoresistance via inducing mitochondrial and liposomal oxidative stress

Mingming Jin (asdjinmingming@126.com)
Shanghai University of Medicine and Healthy Science

Yue Wu
Shanghai University of Medicine and Health Sciences

Yuqing Lou
Shanghai University of Medicine and Health Sciences

Xiyu Liu
Shanghai University of Medicine and Health Sciences

Yitian Dai
Shanghai University of Medicine and Health Sciences

Wenxiao Yang
Shanghai University of Medicine and Health Sciences

Congbiao Liu
Shanghai University of Medicine and Health Sciences

Gang Huang
Shanghai University of Medicine and Health Sciences

Research

Keywords: corosolic acid, non-small cell lung cancer, oxidative stress, apoptosis, chemoresistance

Posted Date: April 9th, 2021

DOI: https://doi.org/10.21203/rs.3.rs-392552/v1

Abstract

Background: Corosolic acid is a pentacyclic triterpenoid isolated from *Lagerstroemia speciosa*, which is known to inhibit cancer cell proliferations. Whereas, it is unclear whether this compound has any effect on non-small cell lung cancer (NSCLC) cells.

Methods: Here, we cultured A549 and PC9 cells in increasing corosolic acid concentrations, as well as treated mice with a physiologically relevant concentration of the compound, and used metabolomics analysis and high-throughput sequencing to examine its influences on cell invasion and proliferation, chemoresistance, and metastasis.

Results: We found that corosolic acid inhibited cell invasion and proliferation *in vivo* and *in vitro*, as well as increase the chemosensitivity of both cell types to cisplatin. Furthermore, we found that corosolic acid destabilized the glutathione peroxidase 2-mediated redox system, which increased mitochondrial and liposomal oxidative stress. Corosolic acid also decreased the targeting protein for Xklp2 level, which inhibited PI3K/AKT signaling and induced apoptosis. In addition, the accumulation of reactive oxygen species dissociated the CCNB1/CDK1 complex and induced G2/M cell cycle arrest.

Conclusion: Taken collectively, the data indicate that corosolic acid reduces NSCLC cell invasion and proliferation, as well as chemoresistance, by inducing mitochondrial and liposomal oxidative stress.

Background

NSCLC is a main cause of cancer-related mortality in US. Currently, overall five-year survival rate of metastatic NSCLC patients is <5% [1]. Although significant advancements have been made in the diagnosis and treatment of NSCLC in the last two decades, more investigations are demanded to unravel the mechanisms underlying the development and progression of NSCLC. Application of small molecule tyrosine kinase inhibitors, combined with immunotherapy, is reported to be successful in patients with NSCLC, especially in those with metastatic disease. Therefore, there is an urgent need for new therapies [1, 2].

Trees and plants are indispensable sources of bioactive compounds that possess anti-cancer properties and exhibit mild side effects [3-5]. Corosolic acid, also known as 2α-hydroxyursolic acid, is a pentacyclic triterpenoid that enriched in the Banaba tree (*Lagerstroemia speciosa*) leaves. Initially, this compound gained attention because of its anti-diabetic properties [6-8]. Subsequently, it was found to possess anti-cancer properties; for instance, corosolic acid can inhibit the development of colorectal cancer through inhibiting HER2/HER3 heterodimerization [8]. In addition, corosolic acid possesses anti-lymphangiogenic and anti-angiogenic properties, as shown in endothelial cells and a colon carcinoma mice model [9]. Corosolic acid is reported to block the transformation and to reactivate Nrf2 in epigenetically-altered TRAMP-C1 prostate cells [10]. However, it is unclear whether this compound has any effect on NSCLC cells. Here, we investigate the corosolic acid effects in lung cancer cells and identify it mechanism of action.

Materials And Methods

Ethics statement

The ethics committee in Shanghai University of Medicine and Health Sciences (Shanghai, China) approved the study protocol.

Cell culture

Our lab purchased A549, PC9, and A549-DDP cells from Type Culture Collection of the Chinese Academy of Sciences (Beijing, China) and cultured them in Dulbecco's Modified Eagle's Medium (Life Technologies, Carlsbad, CA, USA) supplied with penicillin (100 IU/mL), streptomycin (100 μg/mL), and 10% [vol/vol] fetal bovine serum (Life Technologies) at 37°C in humidified atmosphere of 95% [vol/vol] air and 5% [vol/vol] CO_2. Our team utilized cells for different experiments, as indicated below.

RNA isolation and quantitative reverse transcription-polymerase chain reaction (RT-qPCR)

Our lab isolated total RNA from cells and tissues through TRIzol Reagent (Life Technologies) following the instruction. Our lab determined RNA purity and concentration at absorbances of 230, 260, and 280 nm with the NanoDrop ND-1000 UV/VIS Spectrophotometer (Thermo Fisher Scientific, Wilmington, DE, USA). $OD_{260}/_{280}$ and $OD_{260}/_{230}$ ratios of 1.8–2.1 and >1.8 were regarded acceptable. Thereafter, our lab reverse transcribed 1 μg of total RNA into complementary DNA using SuperScript II Reverse Transcriptase (Thermo Fisher Scientific). Our team performed qPCR in an AB 7300 Real-Time System (Applied Biosystems, Foster City, CA, USA) through TaqMan Universal PCR Master Mix (Thermo Fisher Scientific). Target gene expression was determined via $2^{-\Delta\Delta Ct}$ method. The primers utilized for qPCR were following: *Gpx2* 5'-GGTAGATTTCAATACGTTCCGGG-3' (forward) and 5'-TGACAGTTCTCCTGATGTCCAAA-3' (reverse), *Tpx2* 5'-ACCTTGCCCTACTA AGATT-3' (forward) and 5'-AATGTGGCACAGGTTGAGC-3' (reverse), *Casp3* 5'-CATGGAAGCGAATCAATGGACT-3' (forward) and 5'-CTGTACCAGACCGAG ATGTCA-3' (reverse), *Ccnb1* 5'-GACCTGTGTCAGGCTTTCTCTG-3' (forward) and 5'-GGTATTTTGGTCTGACTGCTTGC-3' (reverse), *Cdk1* 5'-GGTTCCTAGTAC TGCAATTCG-3' (forward) and 5'-TTTGCCAGAAATTCGTTTGG-3' (reverse), and *Gapdh* 5'-GCACCGTCAAGGCTGAGAAC-3' (forward) and 5'-GGATCTCGCTCCT GGAAGATG-3' (reverse). *Gapdh* served as the reference gene.

Metabolomics data analysis

We employed A549 cells treated with or not corosolic acid for metabolomics analysis. Our team seeded cells (1×10^6 cells/well) in 6-well plates and cultured for 2 days. Thereafter, we washed cells with phosphate buffered saline (PBS) three times, fixed them with ice-cold methanol, collected them into microcentrifuge tubes, and homogenized them on ice. Our team centrifuged samples at 14,000 × *g* for 10 minutes and analyzed them by liquid chromatography-mass spectrometry. Our team processed data with Compound Discoverer Software (Thermo Fisher Scientific), followed by orthogonal partial least squares discriminant analysis (OPLS-DA) and PCA with SIMCA-P Software (MKS Umetrics AB, Umeå, Sweden).

The metabolite characterization was based upon product ion spectra and accurate masses. We used MetaboAnalyst Software for pathway analysis.

Strand-specific and high-throughput RNA-Seq library construction

Our team extracted total RNA from A549 cells treated with and without corosolic acid as indicated above. To remove ribosomal RNA, the VAHTS Total RNA-seq (H/M/R) Library Prep Kit (Vazyme Biotech Co., Ltd, Nanjing, China) following the instruction. Thereafter, our team treated RNA that purified with RNase R (Vazyme Biotech Co., Ltd, Nanjing, China), followed by purification with TRIzol Reagent. The KAPA Stranded RNA-Seq Library Prep Kit (Roche, Basel, Switzerland) was used to prepare libraries, which were subjected to deep sequencing using the Illumina HiSeq 4000 System (Aksomics, Inc., Shanghai, China).

Cell migration assay

Transwell cell culture inserts (Corning Inc., Corning, NY, USA) were employed for cell migration assay. One day after incubation, cells on upper surfaces of membranes were erased with cotton swabs, whereas our team fixed those on lower surfaces with ice-cold methanol for 10 min and stained them with crystal violet solution. Our team photographed stained cells with an inverted light microscope (Olympus, Tokyo, Japan) and counted them in five randomly selected fields.

Cell cycle analysis and apoptosis assay

For cell cycle analysis, our team labeled cells with propidium iodide (PI). The DNA content was determined with the NovoCyte 2000 Flow Cytometer (Aglilent Technologies, lnc., Brea, CA, USA).

For the apoptosis assay, Annexin V/PI Staining Kit (Abcam, Cambridge, MA, USA) was used. We seeded cells (1×10^3/well) in plates with 96 wells and incubated them with solasonine (15 μg/mL) for 1 day. Thereafter, we trypsinized cells, washed them with PBS, resuspended them in binding buffer, and simultaneously stained them with annexin V-fluorescein isothiocyanate and PI for 15 minutes at room temperature in dark conditions. The apoptotic rate was determined with the NovoCyte 2000 Flow Cytometer.

Wound healing assay

PC9 and A549 cells (1×10^6 cells/well) transfected with corresponding vectors were seeded in 6-well plates and cultured for 1 days until confluence. We generated wounds by scratching cell layers with 100-mL pipet tips, and cells were cultured for an additional 1, 2, and 3 days, as indicated above. Cells were photographed with a light microscope, and images were compared to respective controls.

Ethynyldeoxyuridine analysis

Our team utilized 5-Ethynyl-2´-deoxyuridine (EdU) Detection Kit (RiboBio, Guangzhou, China) to assess cell proliferation. We seeded PC9 and A549 cells (5×10^3 cells/well) in 96-well plates and cultured them

for 1 days until confluence. Thereafter, our team added EdU labeling reagent to each well, and incubated plates for another two hours. We fixed cells with 4% [wt/vol] paraformaldehyde, permeabilized them with 0.5% [vol/vol] Triton X-100, stained them with Hoechst 33342, and viewed them under an inverted fluorescence microscope (Olympus). We calculated EdU incorporation ratio as EdU-stained cell (red fluorescence) numbers over the Hoechst 33342-stained cell (blue fluorescence) numbers.

Cell proliferation assay

We utilized Cell Counting Kit-8 assay (Dojindo Laboratories, Kumamoto, Japan) to assess cell proliferation following the instruction. We seeded cells (1×10^3/well) in 96-well plates containing 100 μL Complete Cell Culture media (Cell Biologics, Inc., Chicago, IL, USA). Absorbance readings were obtained at 570 nm, and the proliferation rate was determined at 1, 2, and 3 days after transfection.

Colony formation assay

We seeded PC9 and A549 cells (1×10^6 cells/well) in 6-well plates, cultured them for 10 days after treated them with corosolic acid for 24 hours. Ten days after treatment, we determined colony number by staining with crystal violet solution and counting stained colonies.

Establishment of tumor mouse model

A549 cells (2×10^6) were resuspended in PBS and injected into the flanks of 4-week-old male nude mice. Five days after injection, mice were randomly divided into 2 groups: (i) control (NC) group received PBS (100 mL) and (ii) corosolic acid treatment group received the compound at 5 mg/kg body weight in 100 mL. We determined tumor volume and body weight every 5 days.

For chemotherapy resistance experiment, A549-DDP cells (2×10^6) were resuspended in PBS and injected into the flanks of 4-week-old male nude mice. Five days after injection, we randomly divided mice into 5 groups: (i) NC group received PBS (100 mL), (ii) the corosolic acid treatment group received the compound at 2.5 mg/kg body weight in 100 mL, (iii) the high DDP treatment group received the compound at 3 mg/kg body weight in 100 mL, (iv) the low DDP treatment group received the compound at 1.5 mg/kg body weight in 100 mL, and (v) the corosolic acid + DDP treatment group received 2.5 mg/kg body weight of the former compound and 1.5 mg/kg body weight of the latter compound in 100 mL. We determined tumor volume and body weight every 5 days.

For tumor metastasis experiment, luminescence-labeled A549 cells (1×10^5) were resuspended in PBS and injected into tail veins of 4-week-old male nude mice. Four weeks after injection, lung metastasis was assessed with a bioluminescence imaging system. The metastatic foci count was determined by hematoxylin and eosin staining of lung tissue cross-sections.

Immunofluorescent staining (IF)

Our team seeded cells on coverslips housed in 6-well plates, fixed with 4% [wt/vol] paraformaldehyde for 20 minutes, and permeabilized with 0.25% [vol/vol] Triton X-100 for 30 minutes. Thereafter, we blocked cells with blocking buffer for 30 minutes and incubated them with a caspase-3 polyclonal antibody overnight at 4°C (1:500, Proteintech Group, Chicago, IL, USA), followed by incubation with secondary antibody for 1 h at room temperature. We stained nuclei with 4',6-diamidino-2-phenylindole (DAPI). Fluorescence was observed with the ImageXpress HT.ai High-Content Imaging System (Molecular Devices, Sunnyvale, CA, USA).

Mitochondrial membrane potential measurement

Our team measured mitochondrial membrane potential with the Mitochondrial Membrane Potential Assay (Beyotime Biotechnology, Shanghai, China). We analyzed cells using the NovoCyte 2000 Flow Cytometer.

Oxidative stress measurement

The MitoSOX Red Mitochondrial Superoxide Indicator (Yeasen Biotech Co., Ltd., Shanghai, China) and the C11 BODIPY581/591 Lipid Peroxidation Sensor (MKBio, Shanghai, China) were used to measure oxidative stress in A549 and PC9 cells. Fluorescence was quantified with the ImageXpress HT.ai High-Content Imaging System.

Statistical analysis

Statistics analysis was conducted with GraphPad Prism Software (GraphPad, San Diego, CA, USA). Statistician determined statistical differences using Student's *t*-test for comparisons between two groups and by ANOVA for comparisons among three or more groups. Data are denoted by means ± standard deviation (SD). *P*-values ≤ 0.05 are regarded statistical significance.

Results

Corosolic acid inhibits NSCLC proliferation

Corosolic acid is known as 2α-hydroxyursolic acid, which has a molecular formula $C_{30}H_{48}O_4$ and a molecular weight 472.70 g/mol (Fig. 1A). In *in vitro* experiments, we found that the proliferation of PC9 and A549 cells decremented dose-dependently after treatment with corosolic acid for 24 hours, with IC_{50} values of 27.5 μg/mL and 12.5 μg/mL, respectively (Fig. 1B, C). Thereafter, we treated A549 cells with 25 and 27.5 μg/mL of corosolic acid and PC9 cells with 10 and 12.5 μg/mL of corosolic acid for 1, 2, and 3 days. Control cells were treated with the vehicle. Concordant with the results in Figure 1B and C, our team found that the A549 and PC9 cell proliferation decremented significantly after corosolic acid treatment at inhibitory concentrations (Fig. 1D, E). EdU analysis revealed that the IC_{50} values for A549 and PC9 cells were 27.5 μg/mL and 12.5 μg/mL, respectively (Fig. 1F–H). Furthermore, we found that the colony number in both cell types after treatment with corosolic acid was lower than that in controls (Fig. 1I–K).

Corosolic acid at inhibitory concentrations incremented the percentage of cells in G2/M phase (22.87% for A549 cells; 33.76% for PC9 cells) compared to controls (16.77% for A549 cells; 26.27% for PC9 cells), nevertheless the percent of cells in S phase was decremented (43.54% for A549 cells; 28.68% for PC9 cells) compared to controls (49.25% for A549 cells; 31.50% for PC9 cells) (Fig. 1L–O).

In *in vivo* experiments, we found that corosolic acid significantly reduced tumor growth, as evidenced by decreased tumor volumes and weights (Fig. 2A–C). By immunofluorescence staining, Ki67 expression was decreased in corosolic acid-treated cells compared to controls (Fig. 2D, E), indicating that corosolic acid can suppress lung cancer cell proliferation.

Corosolic acid inhibits NSCLC cell migration and invasion

We found that the A549 and PC9 cell migration decremented dose-dependently after treatment with corosolic acid for 24 hours, with IC_{50} values of 15 μg/mL and 7.5 μg/mL, respectively (Fig. 3A–C). Furthermore, we found that the invasion of both cell types was decreased after treatment with corosolic acid at inhibitory concentrations (Fig. 3D–G). Hematoxylin and eosin staining of lung tissue cross-sections, coupled with imaging analysis, revealed that corosolic acid decreased the metastatic foci number compared with controls, indicative of decreased pulmonary metastasis (Fig. 4A–D). These results indicate that corosolic acid can inhibit lung cancer cell invasion and migration.

Corosolic acid suppresses NSCLC cell chemoresistance

Flow cytometric analysis revealed that treatment with corosolic acid at inhibitory concentrations for 24 hours induced apoptosis (Fig. 5A–D). The result also found that the apoptosis of A549-DDP cells were increased with the dose increased of cisplatin (Fig. 5E, F). No apoptosis was observed when we treated A549-DDP cells with corosolic acid (5 μg/mL) or cisplatin (6 μg/mL). However, apoptosis was observed when we simultaneously treated A549-DDP cells with both compounds at the indicated concentrations; the percentage of apoptotic cells treated with both compounds increased to 26% compared to controls (Fig. 5G, H). Furthermore, tumor growth was significantly decreased in mice treated with cisplatin (3 mg/kg), as well as in those treated with cisplatin (1.5 mg/kg) and corosolic acid (2.5 mg/kg), but not in mice treated with cisplatin (1.5 mg/kg) or corosolic acid (2.5 mg/kg) (Fig. 5I, J).

Corosolic acid induces mitochondrial and liposomal oxidative stress

We found that corosolic acid increased mitochondrial and liposomal oxidative stress in both A549 (27.5 μg/mL) and PC9 (12.5 μg/mL) cells (Fig. 6A, B), with liposomal oxidative stress triggering ferroptosis in lung cancer cells. By immunofluorecence staining, caspase-3 expression in corosolic acid-treated cells was increased compared to controls (Fig. 6C).

mRNA high-throughput sequencing, metabolomics data collection and analysis

Metabolite analysis revealed that corosolic acid increased the levels of many metabolites, including anatalline, L-carnitine, oxidized glutathione, suberic acid, lysylvaline, acetanilide, and L-arginine, in A549

cells (Fig. 7A, B). We used MetaboAnalyst Software (Fig. 7C) to pinpoint the pathways underlying these alterations in metabolites, and identified several pathways altered by corosolic acid such as glutathione (GSH) metabolism; asminoacyl-tRNA biosynthesis; tyrosine, phenylalanine and tryptophan biosynthesis; and D-glutamine and D-glutamate metabolism. Former investigations reported that disruption of glutathione peroxidase 2-mediated redox reactions can increase oxidized glutathione levels, thereby inducing ferroptosis. Flow cytometric analysis showed the mitochondrial membrane potential of A549 after treatment with 27.5 μg/ml corosolic acid with or without added 1 μM ferrostatin-1. The ferroptosis inhibitor, ferrostatin-1, reversed the corosolic acid-induced depolarization of the mitochondrial membrane potential (Fig. 8A). Furthermore, corosolic acid-induced apoptosis was partly reversed after treatment with ferrostatin-1 (Fig. 8B, C).

By high-throughput sequencing, we found that 1812 and 3441 genes in corosolic acid-treated A549 cells were up- and down-regulated, respectively, compared with controls (supplementary materials. 1). Furthermore, the levels of GPX2, AKT1, TPX2, CCNB1, and CDK1 were decreased after treatment with corosolic acid (Fig. 9A, B), and the data were confirmed via RT-qPCR (Fig. 9C). By RT-qPCR, we also found that corosolic acid increased the caspase-3 level.

Discussion

Despite significant advancements in the NSCLC diagnosis and treatment, the patient prognosis is often unsatisfactory due to metastasis [11], and there is an urgent need for new therapies. Corosolic acid is a pentacyclic triterpene that is enriched in medicinal plants such as *Ugni molinae*, *Vaccinium macrocarpon*, and *Eriobotrya japonica* [12]. Former investigations reported that corosolic acid can inhibit cancer cell proliferation and invasion, as well as chemoresistance [7, 13, 14]. While the corosolic acid effect on lung cancer cells is unknown. Current sutdy found that corosolic acid suppressed lung cancer cell proliferation and invasion dose-dependently, with IC_{50} values of 27.5 μg/mL and 12.5 μg/mL for A549 and PC9 cell migration, and IC_{50} values of 15 μg/ml and 7.5 μg/mL for A549 and PC9 cell invasion. Corosolic acid also halted the cell cycle at G2 phase. Taken collectively, these results indicate that corosolic acid affects cell migration.

Many patients with advanced NSCLC do not respond to treatment, and chemoresistance can be caused by gene alterations, epigenetic alterations, and tumor heterogeneity [15]. Here, the cisplatin-resistant strain, A549-DDP, was used. We found that corosolic acid induced A549 and PC9 cell apoptosis dose-dependently. However, no apoptosis was detected in A549-DDP cells treated with corosolic acid (5 μg/mL) or cisplatin (3 μg/mL), although simultaneous treatment with both compounds promoted apoptosis. These results were confirmed in *in vivo* experiments, which showed that low concentrations of cisplatin and corosolic acid significantly inhibited tumor growth, indicating that corosolic acid can increase the sensitivity of lung cancer cells to drugs.

We performed metabolomics analysis to identify the mechanism of action of corosolic acid. We found that corosolic acid altered glutathione metabolism. Previous studies have reported that glutathione

metabolism limits oxidative stress in cells , and ROS-induced oxidative damage induces ferroptosis [16, 17]. Here, the ROS in A549 cell levels increased after treatment with corosolic acid, whereas ROS production was decreased after treatment with ferrostatin-1.

This study also revealed that corosolic acid can induce mitochondrial oxidative stress and disrupt the mitochondrial membrane potential. Mitochondrial dysfunction can cause apoptosis [18], and the release of sufficient amounts of ROS into the mitochondria vicinity can activate local pools of redox-sensitive enzymes, such as the pro-apoptotic protein, caspase-3 [19, 20]. The results of high-throughput sequencing and RT-qPCR revealed that treatment with corosolic acid decreased the levels of GPX2, AKT1, TPX2, and CCNB1. A previous study has reported that glutathione peroxidases (GPXs) 1–4 can protect against oxidative challenge, thereby inhibiting inflammation and apoptosis by maintaining the redox balance [21]. Corosolic acid decreased the GPX2 level and induced ferroptosis. Other research illustrated that the CCNB1/CDK1 complex dissociation can suppress cell invasion [22, 23], and decreased levels of CCNB1 and CDK1 can induce G2/M cell cycle arrest and promote apoptosis [24]. Here, we found that corosolic acid down-regulated the TPX2 level, which inhibited PI3K/AKT signaling and promoted caspase-3-mediated apoptosis [25]. TPX2, microtubule-associated protein, regulates the dynamics of mitotic spindles, which is indicative of its important role in the cell cycle [26]. In other studies, TPX2 was demonstrated to function as an oncogene, and TPX2 knockdown promoted apoptosis and blocked tumor cell growth [27].

Conclusions

Taken collectively, our results show that corosolic acid destabilized the GPX2- mediated redox system, thereby increasing mitochondrial and liposomal oxidative stress. Corosolic acid also decreased the TPX2 level, inhibiting PI3K/AKT signaling and inducing apoptosis. The accumulation of ROS dissociated the CCNB1/CDK1 complex and induced cell cycle arrest at the G2/M phase, which further promoted apoptosis (Fig. 10). Further mechanistic studies are needed to expand these findings.

List Of Abbreviations

NSCLC, non-small cell lung cancer; RT-qPCR, quantitative reverse transcription-polymerase chain reaction; PBS, phosphate buffered saline; EdU, 5-Ethynyl-2´-deoxyuridine; CCK8, DAPI, Cell Counting Kit-8; 4',6-diamidino-2-phenylindole;

Declarations

Ethics approval and consent to participate

None.

Consent for publication

All authors have agreed to publish this manuscript.

Availability of data and material

The data generated or analyzed during this study are included in this article, or if absent are available from the corresponding author upon reasonable request.

Competing interests

The authors declare that they have no competing interests.

Funding

The study was funded by National Natural Science Foundation of China (nos. 81830052, 82003142, and 81530053), the Shanghai Key Laboratory of Molecular Imaging (no. 18DZ2260400) and the Special Innovative Training Program for Postgraduates (no. Y2020077).

Authors' contributions

MJ, YW, and YL performed research and analyzed results. XL and YD discussed results. WY edited the paper. MJ, CL and GH designed the research and drafted the paper. GH conceived the study. All authors approved the final manuscript.

Acknowledgements

Not applicable.

References

[1] Arbour, K. C.; Riely, G. J. Systemic Therapy for Locally Advanced and Metastatic Non-Small Cell Lung Cancer: A Review. *JAMA* **322:**764-774; 2019.

[2] Reck, M.; Rabe, K. F. Precision Diagnosis and Treatment for Advanced Non-Small-Cell Lung Cancer. *N Engl J Med* **377:**849-861; 2017.

[3] Shinde, P.; Banerjee, P.; Mandhare, A. Marine natural products as source of new drugs: a patent review (2015-2018). *Expert Opin Ther Pat* **29:**283-309; 2019.

[4] Seca, A. M. L.; Pinto, D. Plant Secondary Metabolites as Anticancer Agents: Successes in Clinical Trials and Therapeutic Application. *Int J Mol Sci* **19**; 2018.

[5] Yin, B.; Fang, D. M.; Zhou, X. L.; Gao, F. Natural products as important tyrosine kinase inhibitors. *Eur J Med Chem* **182:**111664; 2019.

[6] Sivakumar, G.; Vail, D. R.; Nair, V.; Medina-Bolivar, F.; Lay, J. O., Jr. Plant-based corosolic acid: future anti-diabetic drug? *Biotechnol J* **4:**1704-1711; 2009.

[7] Jia, M.; Xiong, Y.; Li, M.; Mao, Q. Corosolic Acid Inhibits Cancer Progress Through Inactivating YAP in Hepatocellular Carcinoma. *Oncol Res* **28:**371-383; 2020.

[8] Zhang, B. Y.; Zhang, L.; Chen, Y. M.; Qiao, X.; Zhao, S. L.; Li, P.; Liu, J. F.; Wen, X.; Yang, J. Corosolic acid inhibits colorectal cancer cells growth as a novel HER2/HER3 heterodimerization inhibitor. *Br J Pharmacol*; 2021.

[9] Yoo, K. H.; Park, J. H.; Lee, D. Y.; Hwang-Bo, J.; Baek, N. I.; Chung, I. S. Corosolic Acid Exhibits Anti-angiogenic and Anti-lymphangiogenic Effects on In Vitro Endothelial Cells and on an In Vivo CT-26 Colon Carcinoma Animal Model. *Phytother Res* **29:**714-723; 2015.

[10] Yang, J.; Wu, R.; Li, W.; Gao, L.; Yang, Y.; Li, P.; Kong, A. N. The triterpenoid corosolic acid blocks transformation and epigenetically reactivates Nrf2 in TRAMP-C1 prostate cells. *Mol Carcinog* **57:**512-521; 2018.

[11] Herbst, R. S.; Morgensztern, D.; Boshoff, C. The biology and management of non-small cell lung cancer. *Nature* **553:**446-454; 2018.

[12] Stohs, S. J.; Miller, H.; Kaats, G. R. A review of the efficacy and safety of banaba (Lagerstroemia speciosa L.) and corosolic acid. *Phytother Res* **26:**317-324; 2012.

[13] Woo, S. M.; Seo, S. U.; Min, K. J.; Im, S. S.; Nam, J. O.; Chang, J. S.; Kim, S.; Park, J. W.; Kwon, T. K. Corosolic Acid Induces Non-Apoptotic Cell Death through Generation of Lipid Reactive Oxygen Species Production in Human Renal Carcinoma Caki Cells. *Int J Mol Sci* **19**; 2018.

[14] Park, J. B.; Lee, J. S.; Lee, M. S.; Cha, E. Y.; Kim, S.; Sul, J. Y. Corosolic acid reduces 5FU chemoresistance in human gastric cancer cells by activating AMPK. *Mol Med Rep* **18:**2880-2888; 2018.

[15] Liu, W. J.; Du, Y.; Wen, R.; Yang, M.; Xu, J. Drug resistance to targeted therapeutic strategies in non-small cell lung cancer. *Pharmacol Ther* **206:**107438; 2020.

[16] Xu, Y.; Zhou, X.; Shi, C.; Wang, J.; Wu, Z. alpha-Lipoic acid protects against the oxidative stress and cytotoxicity induced by cadmium in HepG2 cells through regenerating glutathione regulated by glutamate-cysteine ligase. *Toxicol Mech Methods* **25:**596-603; 2015.

[17] Thangavel, S.; Mulet, C. T.; Atluri, V. S. R.; Agudelo, M.; Rosenberg, R.; Devieux, J. G.; Nair, M. P. N. Oxidative Stress in HIV Infection and Alcohol Use: Role of Redox Signals in Modulation of Lipid Rafts and ATP-Binding Cassette Transporters. *Antioxid Redox Signal* **28:**324-337; 2018.

[18] Wu, C.; Zhao, W.; Yu, J.; Li, S.; Lin, L.; Chen, X. Induction of ferroptosis and mitochondrial dysfunction by oxidative stress in PC12 cells. *Sci Rep* **8:**574; 2018.

[19] Zorov, D. B.; Juhaszova, M.; Sollott, S. J. Mitochondrial reactive oxygen species (ROS) and ROS-induced ROS release. *Physiol Rev* **94:**909-950; 2014.

[20] Kang, Z.; Qiao, N.; Liu, G.; Chen, H.; Tang, Z.; Li, Y. Copper-induced apoptosis and autophagy through oxidative stress-mediated mitochondrial dysfunction in male germ cells. *Toxicol In Vitro* **61:**104639; 2019.

[21] Brigelius-Flohe, R.; Flohe, L. Regulatory Phenomena in the Glutathione Peroxidase Superfamily. *Antioxid Redox Signal* **33:**498-516; 2020.

[22] Fang, L.; Du, W. W.; Awan, F. M.; Dong, J.; Yang, B. B. The circular RNA circ-Ccnb1 dissociates Ccnb1/Cdk1 complex suppressing cell invasion and tumorigenesis. *Cancer Lett* **459:**216-226; 2019.

[23] Zou, Y.; Ruan, S.; Jin, L.; Chen, Z.; Han, H.; Zhang, Y.; Jian, Z.; Lin, Y.; Shi, N.; Jin, H. CDK1, CCNB1, and CCNB2 are Prognostic Biomarkers and Correlated with Immune Infiltration in Hepatocellular Carcinoma. *Med Sci Monit* **26:**e925289; 2020.

[24] Park, C.; Cha, H. J.; Lee, H.; Hwang-Bo, H.; Ji, S. Y.; Kim, M. Y.; Hong, S. H.; Jeong, J. W.; Han, M. H.; Choi, S. H.; Jin, C. Y.; Kim, G. Y.; Choi, Y. H. Induction of G2/M Cell Cycle Arrest and Apoptosis by Genistein in Human Bladder Cancer T24 Cells through Inhibition of the ROS-Dependent PI3k/Akt Signal Transduction Pathway. *Antioxidants (Basel)* **8**; 2019.

[25] Huang, D. H.; Jian, J.; Li, S.; Zhang, Y.; Liu, L. Z. TPX2 silencing exerts antitumor effects on hepatocellular carcinoma by regulating the PI3K/AKT signaling pathway. *Int J Mol Med* **44:**2113-2122; 2019.

[26] Fu, J.; Bian, M.; Xin, G.; Deng, Z.; Luo, J.; Guo, X.; Chen, H.; Wang, Y.; Jiang, Q.; Zhang, C. TPX2 phosphorylation maintains metaphase spindle length by regulating microtubule flux. *J Cell Biol* **210:**373-383; 2015.

[27] Long, N.; Chu, L.; Jia, J.; Peng, S.; Gao, Y.; Yang, H.; Yang, Y.; Zhao, Y.; Liu, J. CircPOSTN/miR-361-5p/TPX2 axis regulates cell growth, apoptosis and aerobic glycolysis in glioma cells. *Cancer Cell Int* **20:**374; 2020.

Figures

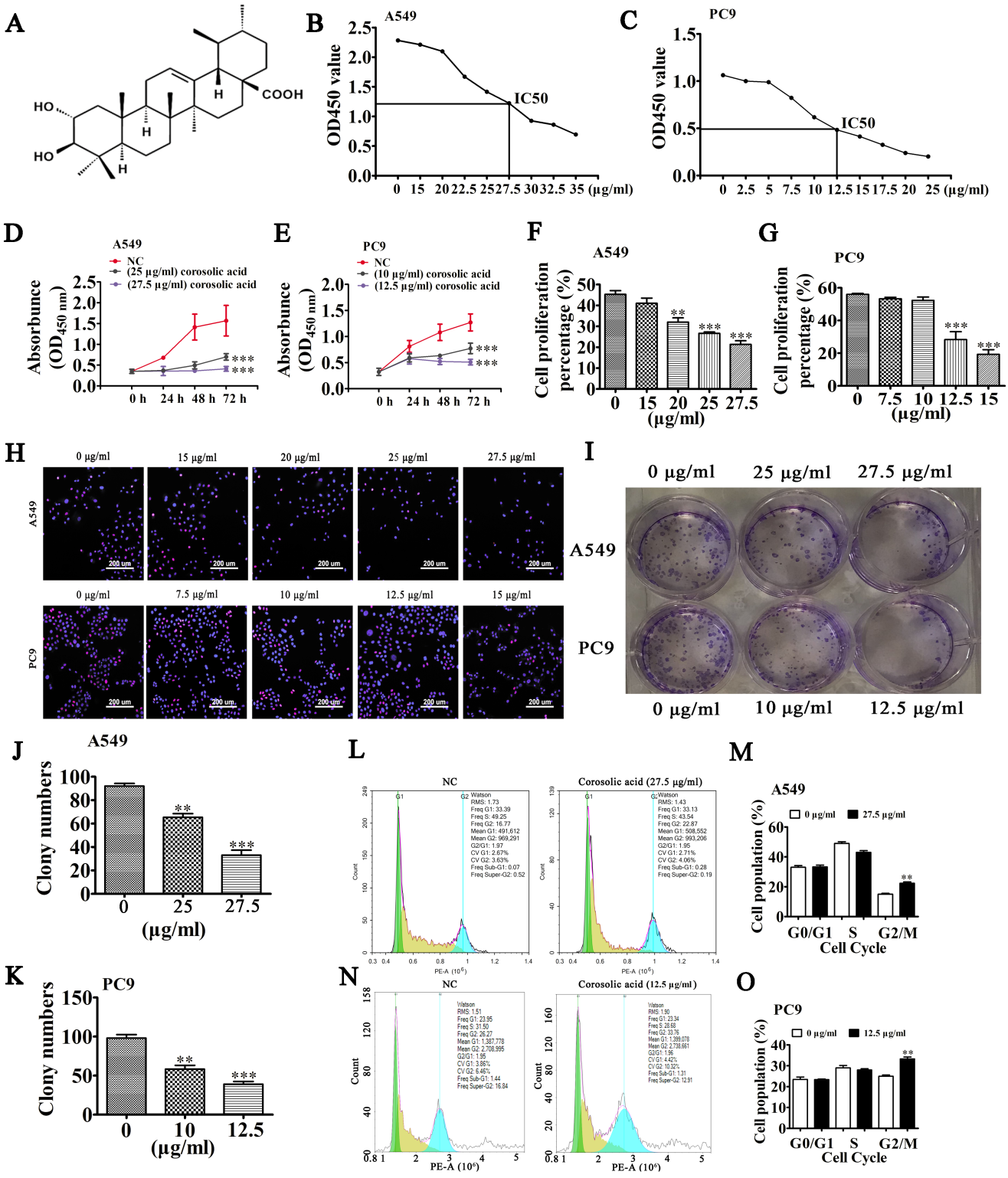

Figure 1

Corosolic acid treatment inhibited the proliferation of human non-small cell lung cancer (NSCLC) cells in vitro. (A) The chemical structure of corosolic acid. (B and C) CCK8 detection of the viability of A549 (B) and PC9 (C) cells after treatment with different concentrations of corosolic acid for 24 h. Data are presented as the mean ± SD. ***p < 0.001 vs. control. OD: optical density. (D and E) The CCK8 assay was used to evaluate the proliferation of both A549 (D) and PC9 (E) cells after treatment with IC50

concentration of corosolic acid for 0, 24, 48 and 72 h. Data are presented as the mean ± SD. **p < 0.01, ***p < 0.001 vs. control. (E-G) Edu assay show the proliferation of both A549 and PC9 cells after treatment with IC50 concentration of corosolic acid for 24 h. Data are presented as the mean ± SD. **p < 0.01, ***p < 0.001 vs. control. (I-K) Cloning formation assay showing the extent of proliferation of both A549 and PC9 cells after pretreatment with IC50 concentration of corosolic acid for 24 h, then cells were culture with normal medium for 10 day. Data are presented as the mean ± SD. **p < 0.01, ***p < 0.001 vs. control. (L) Flow cytometry detection of the percentage of A549 and PC9 cells in the G1, S, or G2 phase. (L-O) Flow cytometry detection of the percentage of A549 and PC9 cells in the G1, S, or G2 phase. Data are presented as the mean ± SD. **p < 0.01 vs. control.

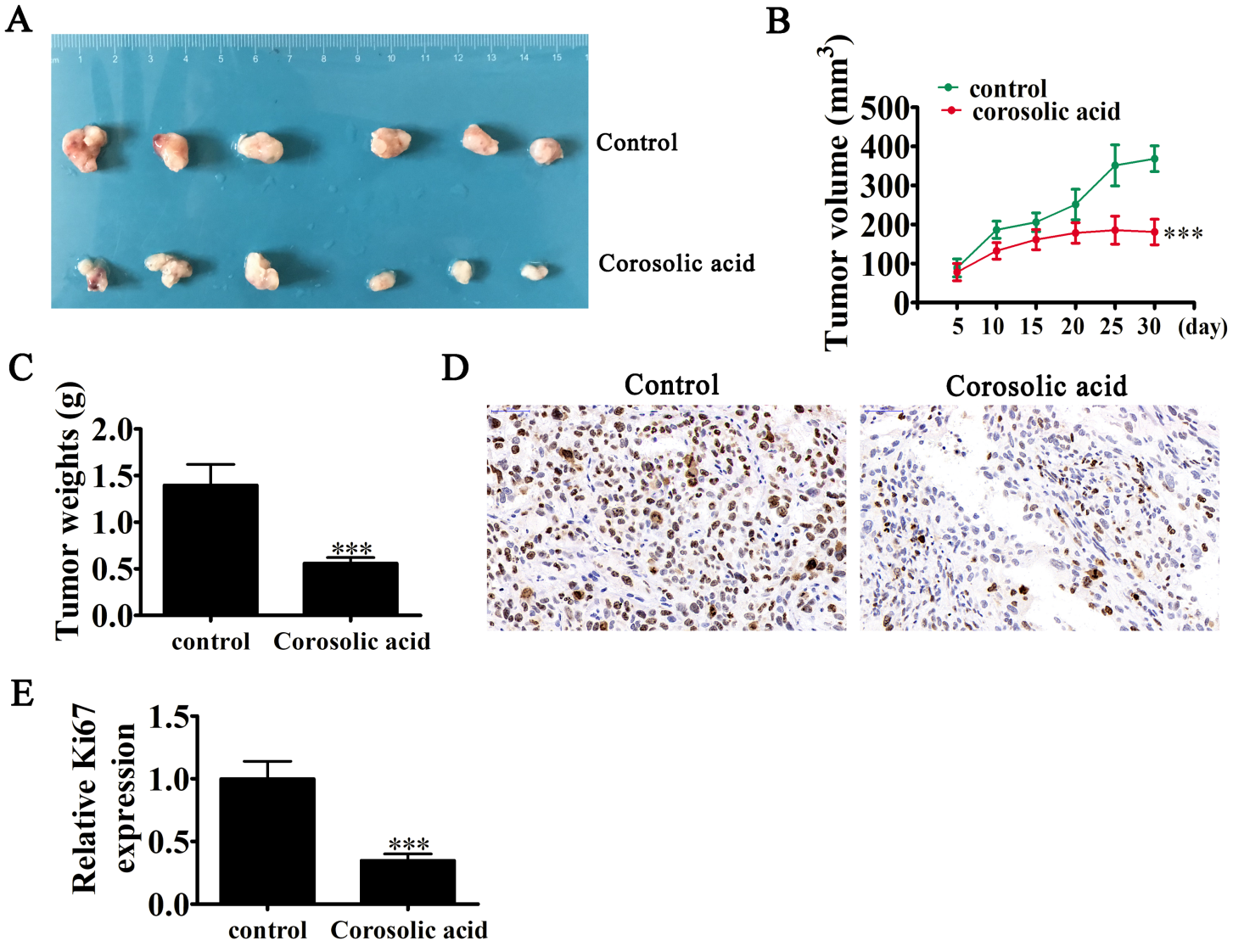

Figure 2

Corosolic acid treatment inhibited the growth of NSCLC cells in vivo. (A) Representative photographs of A549 tumor formation in the xenografts of nude mice. (B) Summary of the tumor volume in mice that were measured every five days. Data are presented as the mean ± SD. ***p < 0.001 vs. control. (C) Tumor weight was measured at 30 days post-injection. Data are presented as the mean ± SD. ***p < 0.001 vs.

control. (D and E) Immunohistochemical analysis showing the percentage of Ki67-positive cells. Data are presented as the mean ± SD. ***p < 0.001 vs. control.

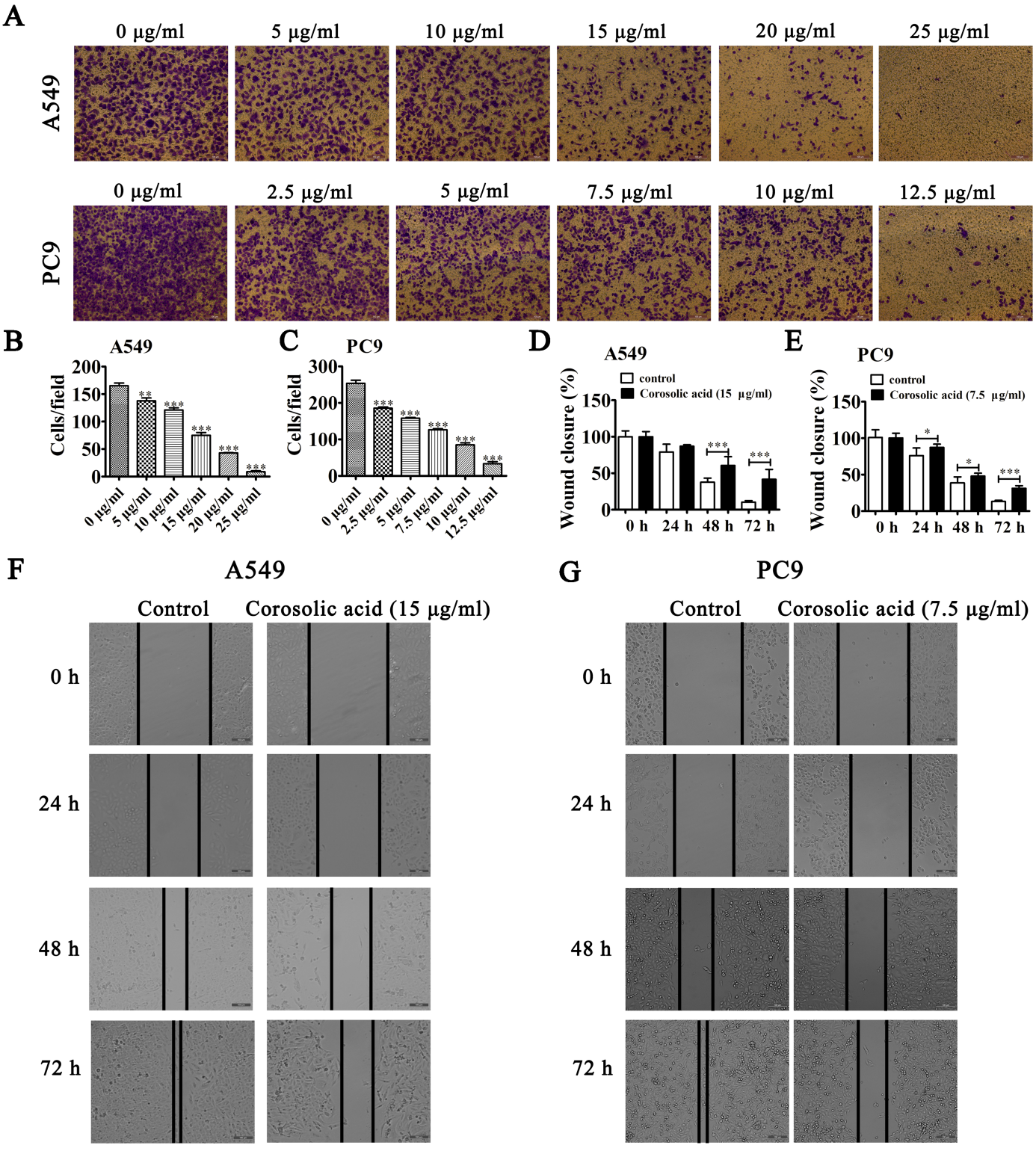

Figure 3

Corosolic acid treatment suppressed NSCLC migration and invasion in vitro. (A-C) Transwell detection show the migration ability of A549 and PC9 cells with different concentrations of corosolic acid treatment for 24 h. Data are presented as the mean ± SD. **p < 0.01, ***p < 0.001 vs. control. (D-G)

Wound-healing assays showing that solasonine suppressed the invasive capacity of both A549 and PC9 cells after treatment with IC50 concentration of corosolic acid for 0, 24, 48 and 72 h. Data are presented as the mean ± SD. *p < 0.05, ***p < 0.001 vs. control.

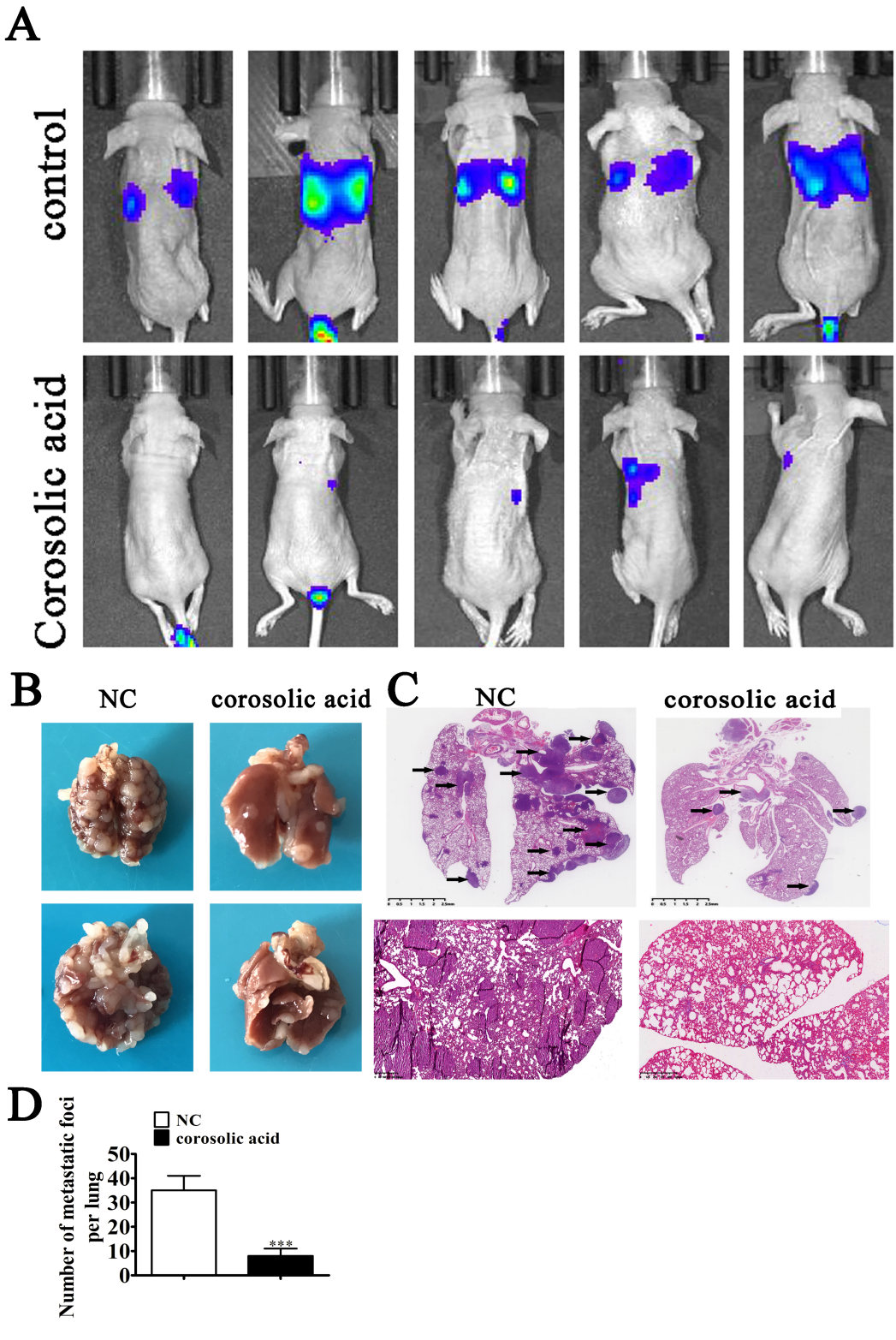

Figure 4

Corosolic acid treatment suppressed A549 invasion in in vivo study. (A) Live imaging showing the effects of corosolic acid on the metastasis of A549 cells 30 d after intravenous tail injection. (B) Metastatic foci

in lung tissues with forward and reverse perspectives. (C and D) The numbers of metastatic foci in lung tissues were caculation according to the HE staining. The data are expressed as the mean ± SD. ***p < 0.001 vs NC.

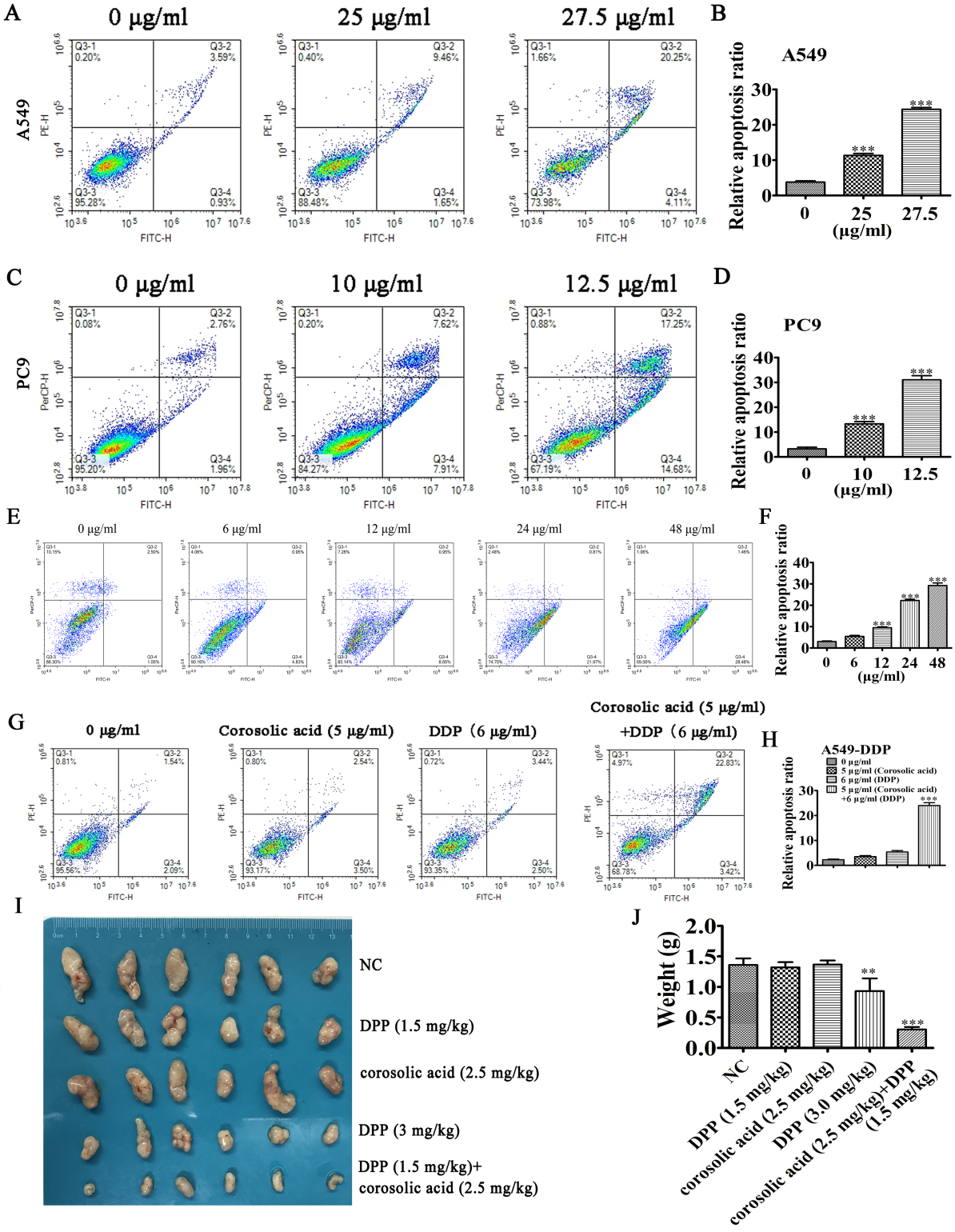

Figure 5

Corosolic acid treatment suppressed NSCLC cells chemotherapy resistance in both in vitro and in vivo. (A-D) Flow cytometry detection show the apoptosis of A549 and PC9 cells after treatment with different

dose of corosolic acid for 24 h. The data are expressed as the mean ± SD. ***p < 0.001 vs control. (E and F) Flow cytometry detection show the apoptosis of A549-DPP cells after treatment with different dose of cis-platinum. Data are presented as the mean ± SD. ***p < 0.001 vs. control. (G and H) Flow cytometry detection show the apoptosis of A549-DPP cells after treatment with cis-platinum and corosolic acid single or combine. Data are presented as the mean ± SD. *p < 0.05, ***p < 0.001 vs. control. (I and J) Representative photographs of A549 tumor formation in the xenografts of nude mice. Tumor weight was measured at 30 days post-injection. Data are presented as the mean ± SD. ***p < 0.001 vs. NC.

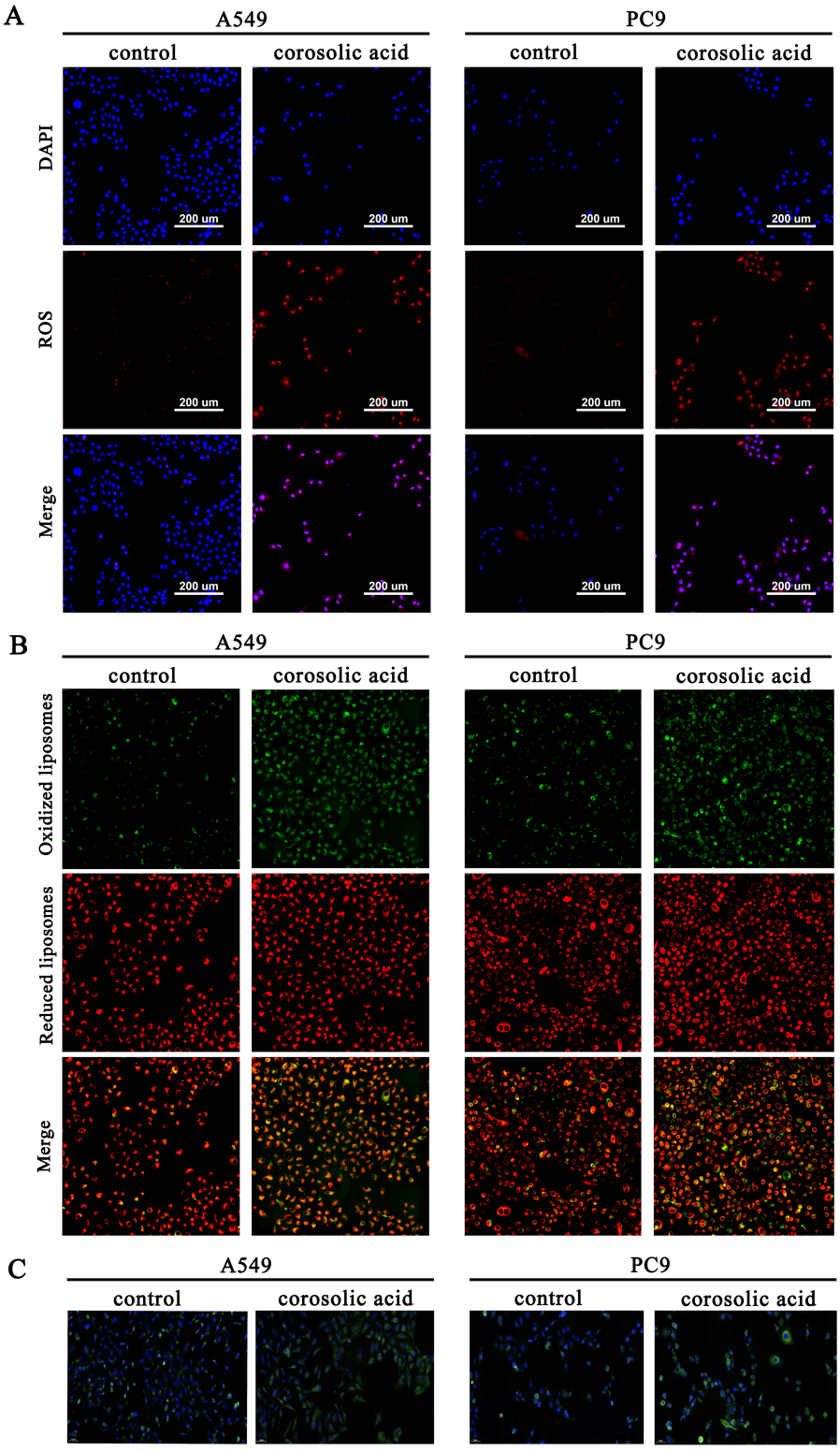

Figure 6

Corosolic acid treatment suppressed NSCLC cells chemotherapy resistance in both in vitro and in vivo. (A-D) Flow cytometry detection show the apoptosis of A549 and PC9 cells after treatment with different dose of corosolic acid for 24 h. The data are expressed as the mean ± SD. ***p < 0.001 vs control. (E and F) Flow cytometry detection show the apoptosis of A549-DPP cells after treatment with different dose of cis-platinum. Data are presented as the mean ± SD. ***p < 0.001 vs. control. (G and H) Flow cytometry detection show the apoptosis of A549-DPP cells after treatment with cis-platinum and corosolic acid single or combine. Data are presented as the mean ± SD. *p < 0.05, ***p < 0.001 vs. control. (I and J) Representative photographs of A549 tumor formation in the xenografts of nude mice. Tumor weight was measured at 30 days post-injection. Data are presented as the mean ± SD. ***p < 0.001 vs. NC.

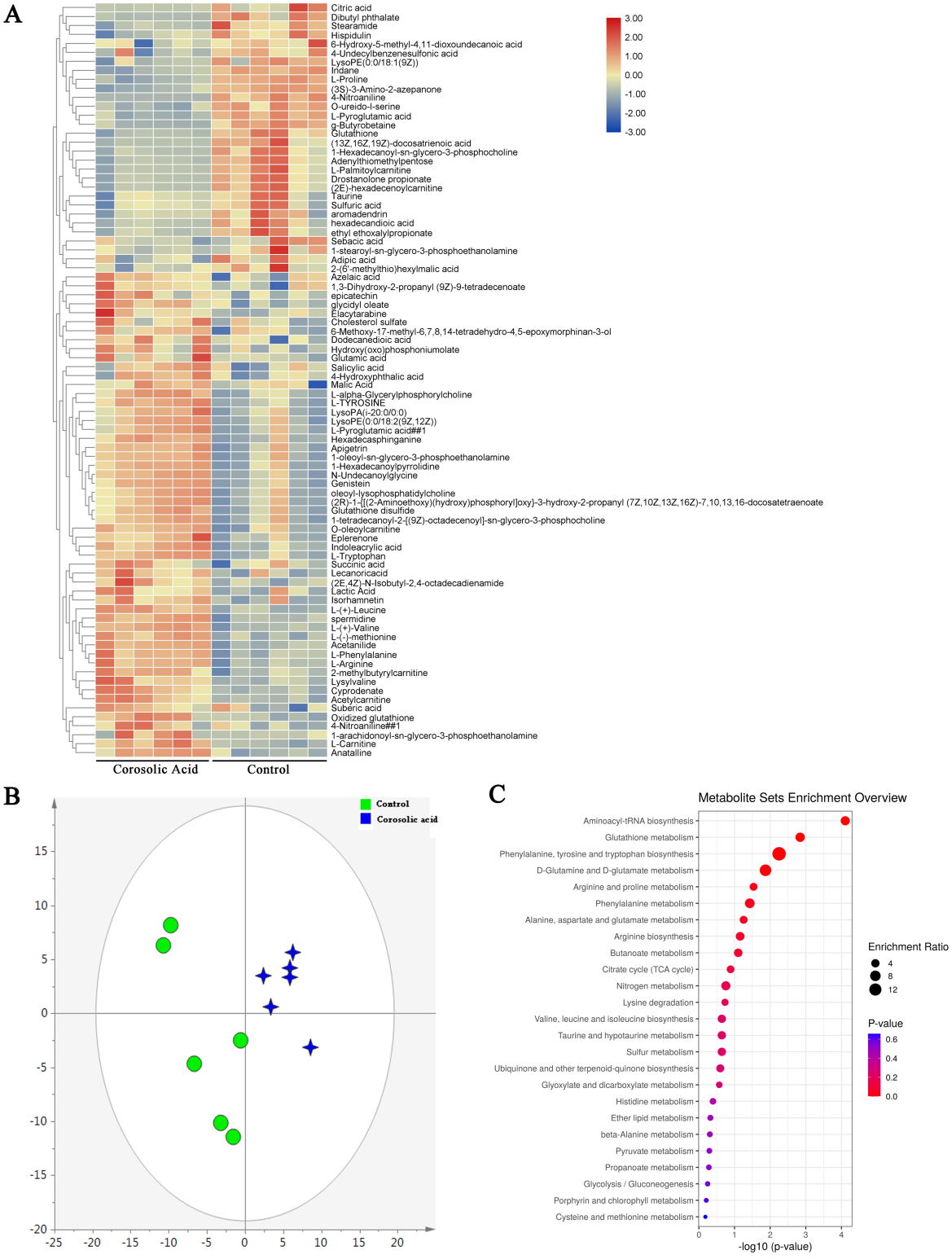

Figure 7

Cell metabolite analysis showing that corosolic acid influenced metabolite production by A549 cells. (A) A heat map was used to identify the metabolite in HepG2 cells. Different colors on the heatmap indicate changes to the metabolite contents, where red indicates a high content, while blue indicates a low content. (B) OPLS-DA score plot showing differences between corosolic acid treatment and control

groups of A549 cells. (C) Pathway analysis of significantly altered metabolites in A549 cells, as compared with baseline.

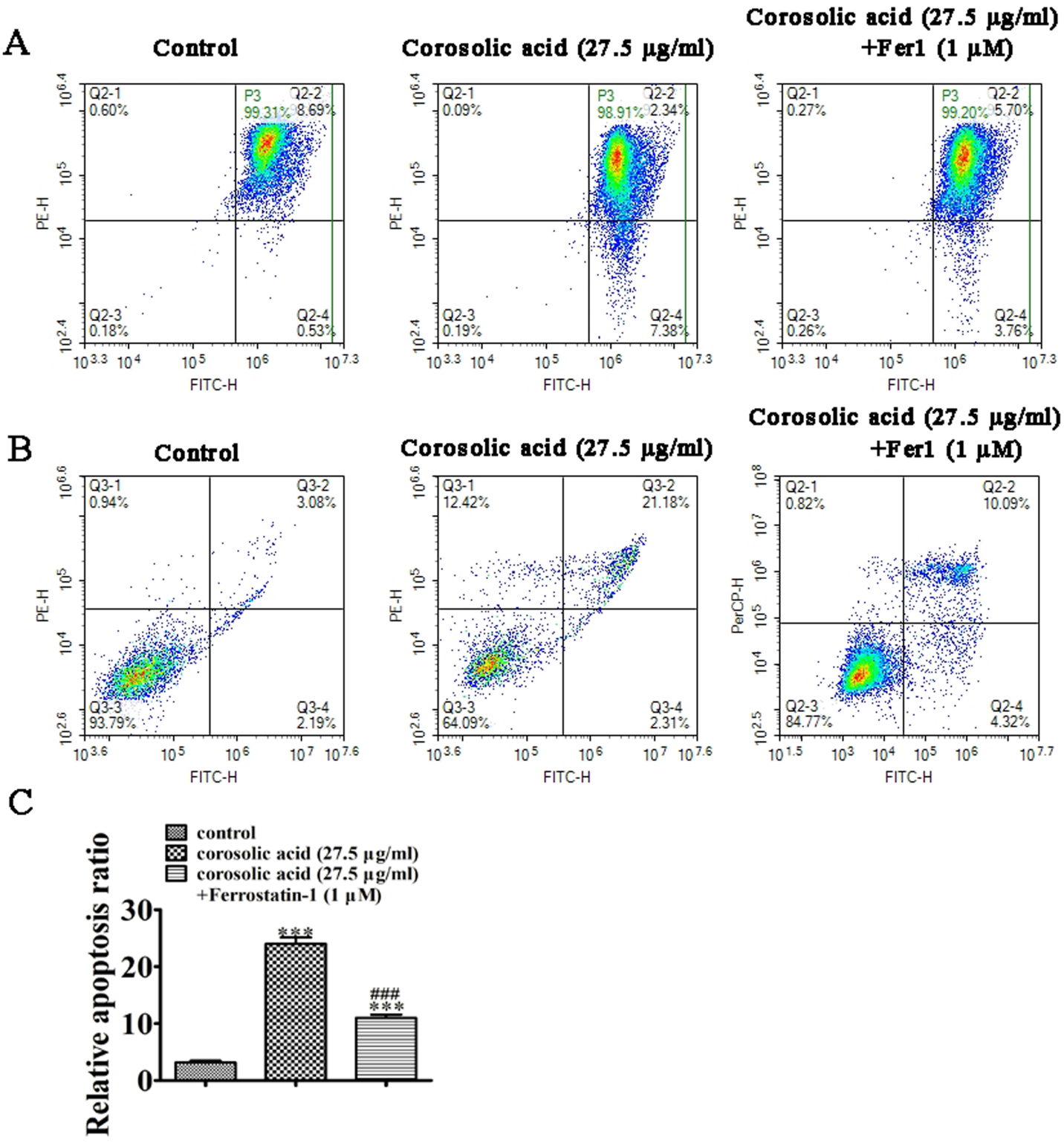

Figure 8

Ferroptosis inhibitor ferrostatin-1 treatment reversed corosolic acid induced A549 apoptosis and depolarization of mitochondrial membrane potential. (A) Flow cytometry detection show the mitochondrial membrane potential of A549. (B) Flow cytometry detection show the apoptosis of A549

after treatment with (27.5 μg/ml) corosolic acid with or without combine ferrostatin-1 (1 μM). Data are presented as the mean ± SD. ***p < 0.001 vs. control. ###p < 0.001 vs. corosolic acid.

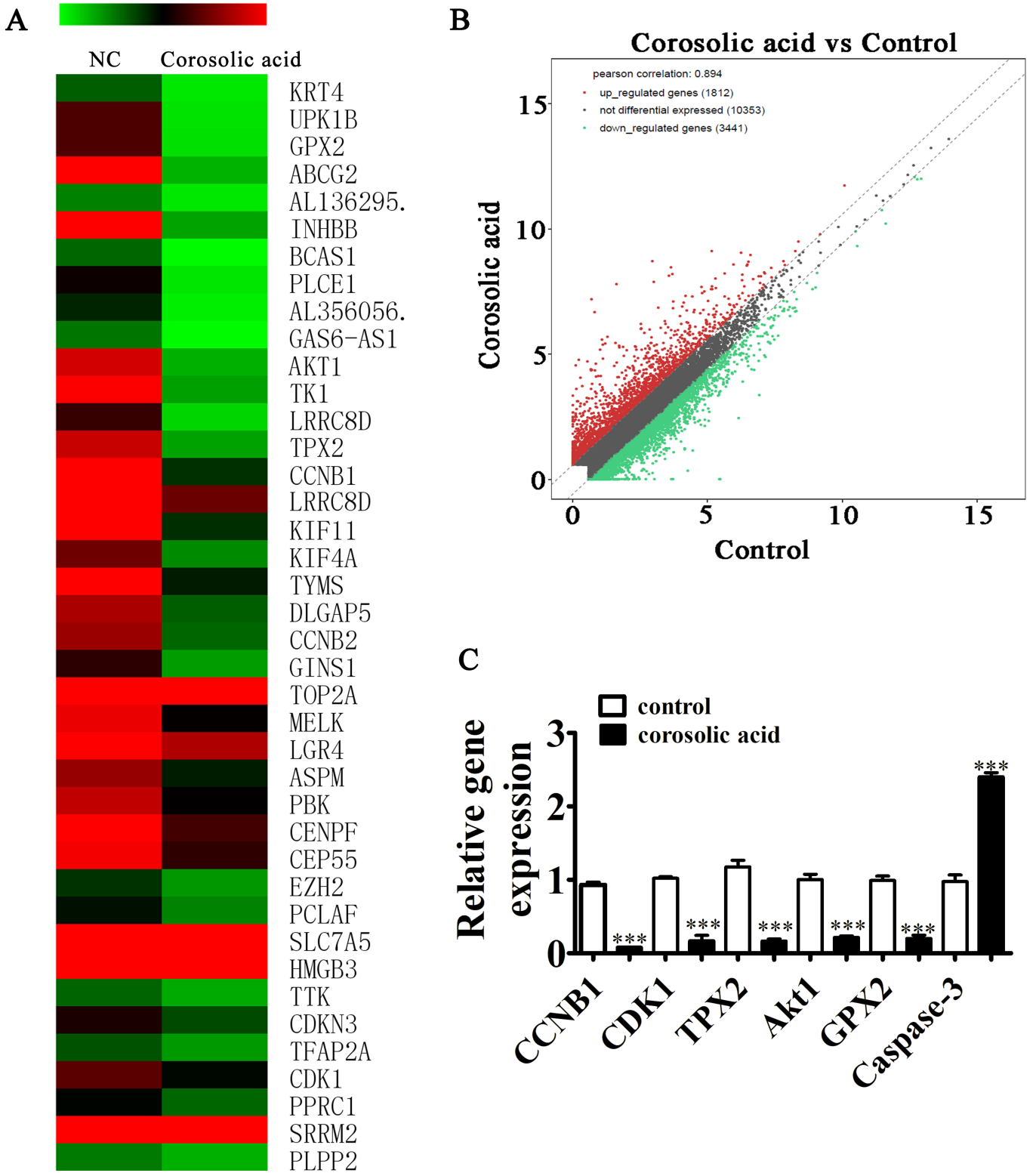

Figure 9

high-throughput sequencing show the different expression of gene after corosolic acid treatment. (A) Clustered heatmap for A549 cells after treatment with corosolic acid when comparted with control cells. (B) Volcano plots illustrated that among significantly different expressed mRNAs, 1812 were upregulated

and 3441 were downregulated in A549 cells after treatment with Corosolic acid when comparted with control cells. (C) RT-qPCR detection show the differentially expressed genes. Data are presented as the mean ± SD. ***p < 0.001 vs. control.

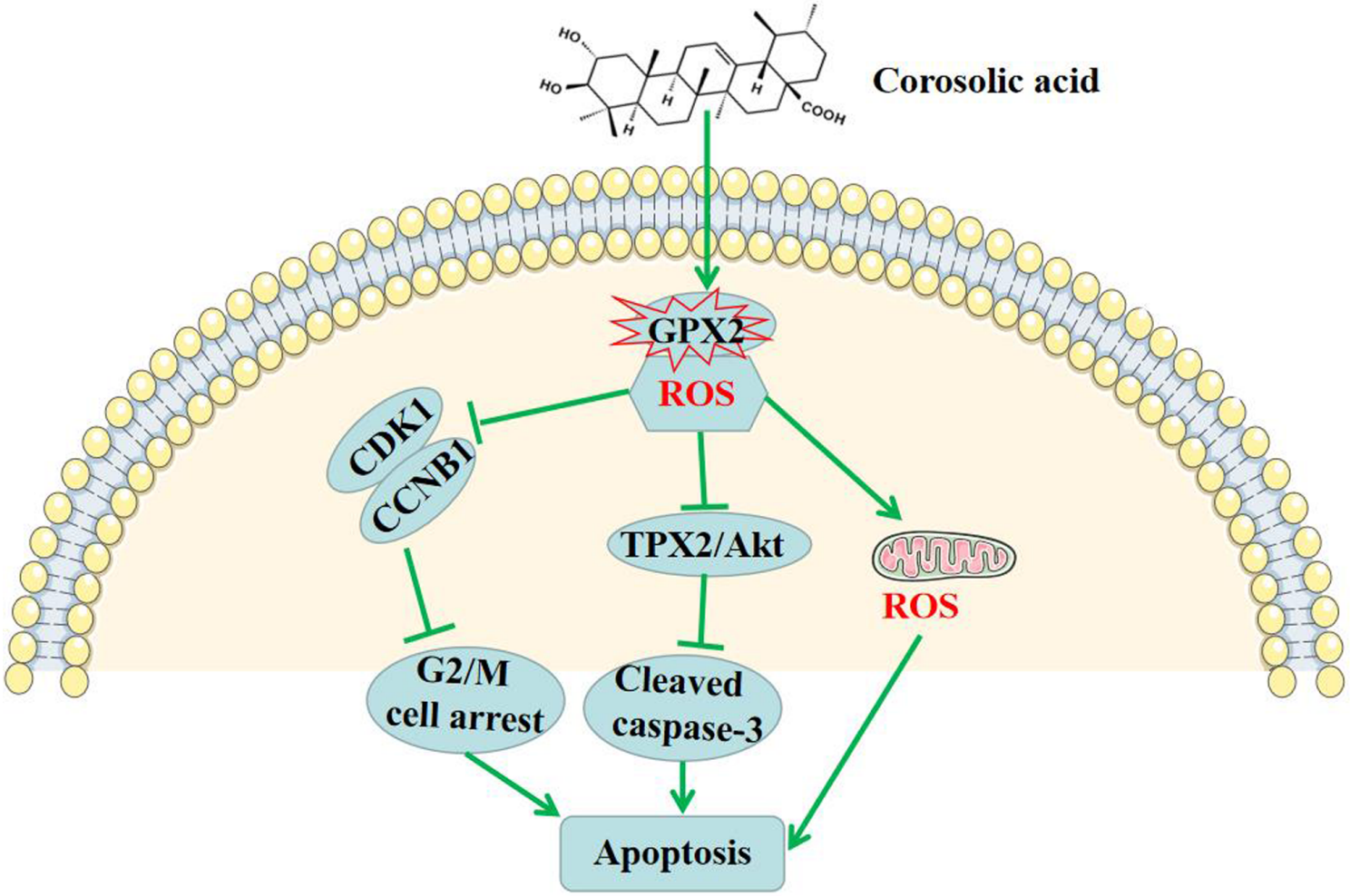

Figure 10

A proposed mechanism of Corosolic acid-induced apoptosis in NSCLC cells.

Supplementary Files

This is a list of supplementary files associated with this preprint. Click to download.

- Supplementarymaterials.1.xlsx